Predicting spread of Alzheimer's disease pathology using brain connectomes from different cognitive stages

Melina Jingting binti Laimon

Abstract

1 Introduction

Alzheimer's disease (AD) is a progressive neurodegenerative disorder and the leading cause of dementia worldwide, affecting tens of millions of people and placing an enormous burden on public health (Yu et al., 2021). Pathologically, AD is characterized by the accumulation of amyloid-β (Aβ) plaques and tau protein neurofibrillary tangles, which disrupt synaptic function and ultimately drive extensive neuronal loss (Goedert, 2015; Weickenmeier et al., 2019). Despite concerted research efforts, effective disease-modifying treatments remain elusive, in part owing to the complexity and heterogeneity of AD progression (Yu et al., 2021). Enhanced mechanistic understanding of how tau pathology spreads, and how Aβ may trigger or accelerate this spread, is therefore crucial for developing earlier diagnostic strategies and more effective interventions.

Tau-propagation models are often based on the **prion hypothesis**, based on evidence indicates that misfolded proteins such as tau propagate trans-synaptically in a prion-like fashion from vulnerable epicenters to connected brain regions, giving rise to the characteristic Braak staging patterns documented in pathological and PET imaging studies (Vogel et al., 2023; Raj et al., 2012). Researchers have thus increasingly turned to *network-based* computational models—relying on connectomics—to better understand how tau spreads via large-scale anatomical or functional pathways in the brain (Raj et al., 2012; **?**; Weickenmeier et al., 2019; He et al., 2023; **?**).

The amyloid cascade hypothesis posits that pathological aggregation of Aβ initiates a cascade culminating in tau-mediated neurodegeneration (Goedert, 2015). Indeed, early Aβ deposition correlates with downstream metabolic and cellular changes that promote tau seeding and aggregation. This synergy helps to explain why tau pathology emerges in close spatiotemporal association with cortical amyloid burden (Biel et al., 2022).

Predictive accuracy of models across cognitive stages is unclear. a pivotal question in these modeling efforts is whether to employ template (group-averaged) connectomes or patient-specific connectomes (**?**Váša and Mišić, 2022). Although group-level templates can simplify modeling and reduce noise, each individual's connectome exhibits unique topological features that might shape disease spread. Meanwhile, most existing approaches apply a single model across heterogeneous cohorts or focus only on one disease stage. Consequently, it remains unclear whether predictive accuracy differ between early asymptomatic or mild cognitive impairment (MCI) stages versus frank AD dementia (He et al., 2023). Moreover, standard network diffusion models often ignore local factors, such as amyloid load, that can modulate tau progression.

To address these gaps, we systematically compare three models for predicting tau spread across the Alzheimer's disease spectrum. Specifically, we evaluate the performance of Network Diffusion Model (NDM), Fisher–Kolmogorov–Petrovsky–Piscounov (FKPP), and a weighted FKPP model that incorporates regional Aβ burden in connectomes derived from participants across four cognitive stages: cognitively normal (CN), early MCI (EMCI), late MCI (LMCI), and probable AD (AD). By examining how each model performs at each

disease stage, we aim to provide insights into the mechanisms and predictive power of network-based disease spread models, as well as clarify the role of amyloid-tau interactions in shaping the topography of tau deposition (Thompson et al., 2024). In doing so, we seek a more comprehensive perspective on AD progression across the clinical continuum and a foundation for future personalized modeling efforts.

2 Methods

2.1 Data

2.1.1 Connectomes

We used structural connectomes for 168 participants in the Alzheimer's Disease Neuroimaging Initiative (ADNI)[1] database, evenly distributed across four cognitive stages: cognitively normal (CN), early mild cognitive impairment (EMCI), late mild cognitive impairment (LMCI), and probable Alzheimer's disease (AD). Each group thus contained 42 participants. For each individual, diffusion MRI and tractography were used to reconstruct whole-brain white matter fibers and generate a weighted, undirected connectivity matrix (Oxtoby et al., 2017). These matrices have node labels corresponding to cortical (and some subcortical) regions of interest, following a predefined parcellation scheme, and edge weights representing the number of streamlines between each pair of regions.

2.1.2 Tau PET data

We used tau PET scans from 242 ADNI participants who were classified as having elevated tau levels. We used group-averaged tau PET signals by averaging SUVR values across 242 individuals. These aggregated tau maps served as the "ground truth" against which we fit our various disease-spread models.

2.1.3 Amyloid PET data

We also incorporated group-averaged amyloid-beta (Aβ) measures (SUVRs) from 241 participants. Amyloid burden is widely believed to initiate upstream in the pathological cascade, potentially catalyzing or accelerating tau aggregation (He et al., 2023; Weickenmeier et al., 2019). We therefore leveraged these Aβ SUVR values to weight the local production term in our Aβ-FKPP model (see Section **??**). For subcortical regions, the amyloid PET intensities have been set to 1 (i.e., no additional weighting) to account for inaccuracies in measuring Aβ in deep structures.

[1] https://adni.loni.usc.edu

2.2 Connectome Metrics using the Brain Connectivity Toolbox

For each individual's structural connectome, we computed all metrics listed below using the Python implementation of the Brain Connectivity Toolbox (BCT).

Before calculating the metrics, each connectome matrix was min-max normalized. This normalization was applied to ensure that differences in overall connection strength between individuals did not bias the graph metrics, allowing for more valid comparisons across participants and groups. We verified that all metrics were computed using weighted undirected versions of the functions in BCT.

For node-level metrics, specifically, node strength and clustering coefficient, we compared the mean values across all nodes as well as conducted between-node analyses. With a large number of 84 nodes, we focus the comparisons made by first conducting Kruskal–Wallis tests across all nodes, and then performing Dunn's post-hoc tests only on the single node with the lowest KW p-value. Statistical tests are elaborated in Section 2.2.2.

2.2.1 Metrics

- **Node strength**: The sum of the weights of all edges connected to a node. This indicates how strongly connected or "well-networked" a region is within the connectome. Nodes with high strength serve as hubs. In the context of pathology, such hubs could accumulate tau from multiple inputs or facilitate its wide dissemination to other regions due to their numerous strong connections.

- **Clustering coefficient**: The fraction of a node's neighbors that are also interconnected with each other. This measures the prevalence of tightly knit clusters (triangles) in the network around that node. This local interconnectedness might influence tau propagation by creating short loops for re-circulating or amplifying tau in a region's vicinity.

- **Global efficiency**: The average of the inverse shortest path lengths between all pairs of nodes. This reflects how efficiently information (or in this case, a spreading agent like tau) can be transferred across the whole brain network.
- **Diffusion efficiency**: The inverse of the mean first-passage time for a random walker to travel between nodes on the network. This quantifies how quickly, on average, a signal (or tau protein) can reach any region from any other region via the connectome.
- **Density**: The ratio of existing edges to possible edges in the network, ignoring weights. A higher density implies more pathways along which tau pathology can travel.

2.2.2 Statistical test

We used the Kruskal-Wallis test as implemented in Scipy[2] to assess whether the distributions of each connectome metric differed significantly across the four cognitive groups. This non-parametric test is appropriate given the non-normality of our data. We then performed Dunn's post-hoc tests as implemented in Scikit-learn[3] to identify which specific groups differed from each other, applying a Bonferroni correction for multiple comparisons.

2.3 Tau Propagation Models using the Network Spreading Models Toolbox

We modelled connectivity-mediated tau propagation using the Network Spreading Models (NSM) Toolbox (Thompson et al., 2024), using specifically the toolbox's implementation of the models NDM, FKPP, weighted FKPP and model selection metric AICc.

2.3.1 Models

- **NDM**: We use the network diffusion model (NDM) as the baseline. NDM as proposed in Raj et al. (2012) models the prion-like diffusion of tau based on connectivity. The model is defined as:

$$\frac{d\mathbf{x}(t)}{dt} = -\beta H \mathbf{x}(t)$$

where $\mathbf{x}(t)$ is the regional pathology at time t, β is the diffusion constant, and H connectome Laplacian. We set the diffusion constant β to 1, since we are not calibrating the model to any specific time scale.

- **FKPP**: The Fisher-Kolmogoroc-Petrovsky-Piscounov FKPP (Weickenmeier et al., 2019) couples diffusive propagation of tau with local logistic growth, and is expressed as:

$$\frac{d\mathbf{x}(t)}{dt} = -\alpha H \mathbf{x}(t) + (1-\alpha)\mathbf{x}(t)(1-\mathbf{x}(t))$$

Where α is the weight for spread contribution.

- **Weighted-FKPP**: The Weighted-FKPP extends the basic FKPP equation by allowing for differing tau production levels at each node (He et al., 2023). In our case, we scale the local growth term according to the local amyloid-β (Aβ) level. For the rest of this paper, we will refer to this model as the **Aβ-FKPP**.

$$\frac{d\mathbf{x}(t)}{dt} = -\alpha H \mathbf{x}(t) + \mathbf{v}(1-\alpha)\mathbf{x}(t)(1-\mathbf{x}(t))$$

where $\mathbf{v}$ is a vector of regional production weights, and is set to be the local Aβ level.

2.3.2 Hyperparameter optimization

There are two key hyperparameters for these models: the seed region and the timepoint. The set of candidate seed regions is constrained to be hemisphere-agnostic, thereby reducing the number of nodes from 84 to 42. The candidate timepoints are defined within the range 0 to 50 in increments of 0.1, over which the model's performance is evaluated.

In the Network Diffusion Model (NDM), the NSM Toolbox identifies the optimal seed region and timepoint via a grid search. In contrast, for the FKPP and Weighted-FKPP models, optimal α and seed are determined using Bayesian optimization with Gaussian Processes. In this approach, the objective function is defined as the sum of squared errors (SSE) between the model's output and the target data, evaluated at the optimal timepoint (i.e. the timepoint that minimizes the SSE).

2.4 Model Selection

We compare the performance of the three models using the following metrics:

[2] https://scipy.org/
[3] https://scikit-learn.org/

- **Sum of Squared Errors (SSE)**: The SSE quantifies the discrepancy between the predicted and observed tau levels. It is defined as:

$$SSE = \sum_{i=1}^{n} (y_i - \hat{y}_i)^2$$

where y_i is the observed tau level, $\hat{y}_i$ is the predicted tau level, and n is the number of regions.

- **Pearson's Correlation Coefficient (r)**: We are also interested in measuring how well a model captures relative distribution of tau across regions. To do so, we compute the Pearson's correlation coefficient, defined as:

$$r = \frac{\sum_{i=1}^{n}(y_i - \bar{y})(\hat{y}_i - \bar{\hat{y}})}{\sqrt{\sum_{i=1}^{n}(y_i - \bar{y})^2}\sqrt{\sum_{i=1}^{n}(\hat{y}_i - \bar{\hat{y}})^2}}$$

where $\bar{y}$ and $\bar{\hat{y}}$ are the means of the observed and predicted tau levels, respectively.

- **Akaike Information Criterion corrected (AICc)**: AIC measures relative quality of a statistical model for a given dataset, balancing goodness-of-fit with model complexity, penalizing models with more parameters. Lower AIC values indicate a better fit. It is defined as:

$$AIC = 2k - 2\ln(L)$$

where k is the number of parameters in the model and L is the likelihood of the model given the data.

AICc is a version of AIC that includes a correction for small sample sizes. It is defined as:

$$AICc = AIC + \frac{2k(k+1)}{n-k-1}$$

where n is the sample size.

In our comparisons, k is set to 2 for NDM (for seed and timepoint) and 3 for FKPP and Aβ-FKPP (for the additional α). Here, we have simply taken each hyperparameter or parameter as an additional degree of freedom. To our best knowledge, there is no existing literature guiding parameter counting when considering a mix of discrete and continuous data. We did not consider v in the Aβ-FKPP as an additional degree of freedom since this is prescribed as Aβ levels.

- **AICc weights**: These weights are derived from the AICc values and represent the relative probability of each model's ability to minimize information loss. They are calculated as:

$$w_i = \frac{e^{-\frac{1}{2}(\Delta AICc_i)}}{\sum_{j=1}^{m} e^{-\frac{1}{2}(\Delta AICc_j)}}$$

where $\Delta AICc_i = AICc_i - \min(AICc)$, and m is the number of models. The weights sum to 1 across all models, allowing for direct comparison of their relative likelihoods.

2.5 Robustness testing by fitting to individual connectomes

To assess model stability, we extended our optimization procedure from group-averaged to individual participant connectomes. For all models, we maintained the group-averaged tau levels as target data (Section 2.1.2) and, for Aβ-FKPP, the group-averaged Aβ levels, acknowledging the limitations of this approach. We calculated the mean and 95 percentile range of SSE and r values across all participants. A robust model should exhibit minimal discrepancy between its performance on average connectomes and the mean performance across individual connectomes, along with a narrow percentile range. This approach distinguishes truly generalizable models from those whose performance may be artificially enhanced by connectome averaging.

2.5.1 Seed Subset Selection

When optimizing across individual connectomes, we used a subset of 5 candidate seeds, by first running the FKPP and Aβ-FKPP models on the first 10 connectomes from each cognitive group. We then selected all the optimal seeds found from these 40 connectomes, namely:

- Inferiortemporal
- Temporalpole
- Amygdala
- Entorhinal
- Middletemporal (included in FKPP only)

2.6 Verifying performance gain factors with null models

2.6.1 Amyloid-β maps

We verify the performance gains of our models from incorporating amyloid-beta and using the best performing cognitive group by conducting permutation tests against models trained on permuted amyloid-beta maps and rewired connectomes respectively.

2.6.2 Best performing group-averaged connectome

We will observe in Section 3.2 that connectome properties such as global efficiency, node strength distribution and clustering coefficient distribution can vary significantly across cognitive groups. We use a null model to verify that the improvements of models are a consequence of the specific connectome configuration of the best performing group-averaged connectome and not merely achieved by their graph properties. We generated 100 randomised connectomes for the best performing group-averaged connectome by iteratively rewiring them using the Brain Connectivity Toolbox[4], with each matrix element rewired approximately ten times. Connectomes are rewired by randomly swapping pairs of edges to preserve the degree distribution of the network (Váša and Mišić, 2022).

3 Results

3.1 Qualitative observations on connectome properties

We first inspected the connectome matrix of a clinically normal individual for an overview of typical connectivity patterns (Figure 1). Interhemispheric edges appear sparser than intrahemispheric connections, in line with known neuroanatomical pathways mostly confined to one hemisphere except for crossing through the corpus callosum. The cerebellum cortex exhibits relatively strong cross-hemisphere connections, likely attributable to the bilateral layout of cerebellar peduncles.

[4] https://pypi.org/project/bctpy/

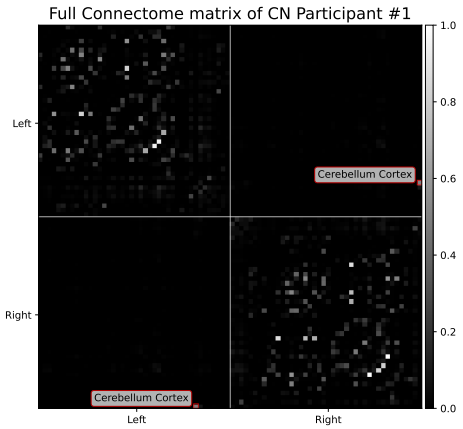

Figure 1: Full connectome matrix.

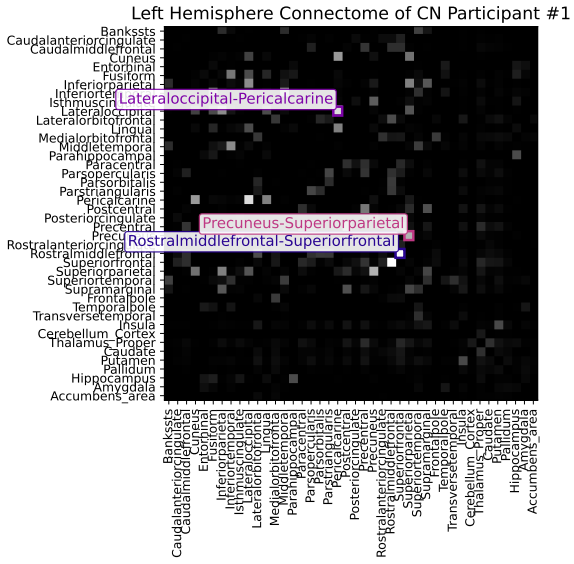

(a) Left hemisphere.

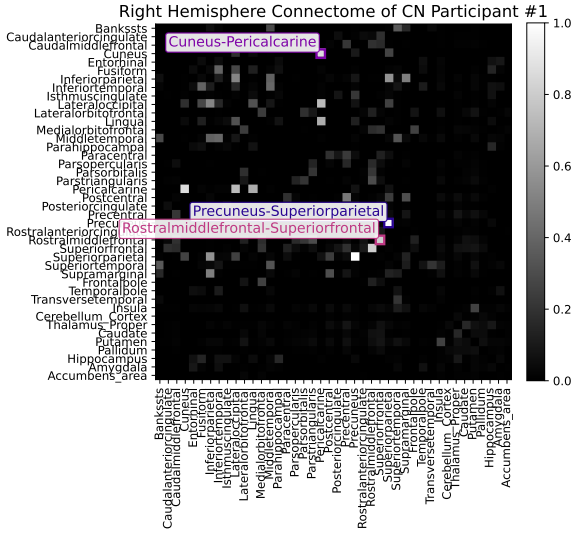

(b) Right hemisphere.

Figure 2: Combined connectome visualisations for a clinically normal participant.

We then observed intra-hemispheric connectivity. Within the left hemisphere (Figure 2a), the strongest edges link Cuneus-Pericalcarine, Precuneus-Superiorparietal and Postcentral-Precentral. We observe similar patterns in the right hemisphere (Figure 2b), with strongest edges connecting Rostralmiddlefrontal-Superiorfrontal, Cuneus-Pericalcarine and Precuneus-Superiorparietal.

3.2 Connectome properties vary across different cognitive stages

We compared the connectome metrics as mentioned in Section 2.2.1. We comment below on the metrics that show significant differences in the Dunn posthoc tests.

- **Global Efficiency**: Shows significant decline (p=0.0073) as cognitive impairment progresses, with particularly strong differences between CN and AD groups (**). This suggests diminishing network integration capacity with disease progression.

- **Node Strength (Right-Hippocampus)**: Displays the strongest statistical significance (p<0.0001) with clear stepwise decline from CN to AD, marked by multiple significant pairwise comparisons (**). This aligns

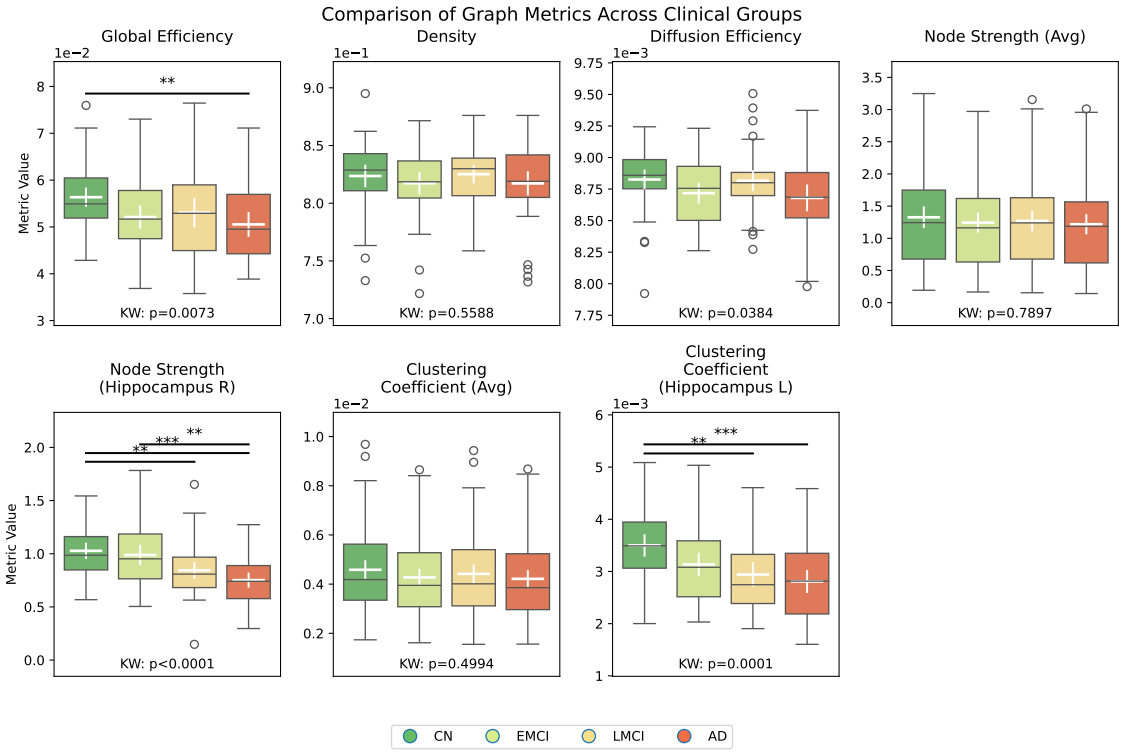

Figure 3: Connectome metrics for different cognitive stages. White horizontal lines indicate the group mean and vertical lines indicate the 95% confidence intervals. Kruskal-Wallis p-values are annotated at the bottom and pairwise differences are computed using Dunn's post-hoc test. Significance indicators: * denotes p < 0.05, ** denotes p < 0.01, and *** denotes p < 0.001.

Table 1: Significant pairwise comparisons between clinical groups

Metric	Group 1	Group 2	Mean 1	Mean 2	% Diff	p-value
Global Efficiency	CN	DEM	5.64e-02	5.05e-02	-10.3%	0.004
Node Strength (Hippocampus R)	CN	LMCI	1.03e+00	8.43e-01	-17.9%	0.005
Node Strength (Hippocampus R)	CN	DEM	1.03e+00	7.52e-01	-26.8%	<0.001
Node Strength (Hippocampus R)	EMCI	DEM	9.88e-01	7.52e-01	-23.9%	0.001
Clustering Coefficient (Hippocampus L)	CN	LMCI	3.50e-03	2.94e-03	-15.9%	0.002
Clustering Coefficient (Hippocampus L)	CN	DEM	3.50e-03	2.81e-03	-19.7%	<0.001

with known hippocampal vulnerability in Alzheimer's disease.

- **Clustering Coefficient (Left-Hippocampus)**: Shows significant differences (p=0.0001) with a pronounced decrease in the AD group, indicating reduced local connectivity in this key memory-related region.

3.3 Model performance

In terms of Pearson's r values, the NDM model performs best, followed by Aβ-FKPP and FKPP. This indicates that NDM is more capable of capturing relative distribution of tau SUVR values across regions. We further probe this in Section 3.3.2.

However, when comparing the models in terms of SSE, AICc and AIC, the Aβ-FKPP model outperforms the other two models. This suggests that the Aβ-FKPP model is better at capturing the overall spread of tau pathology, and supports the hypothesis of Aβ-modulated tau accumulation.

3.3.1 Predicted seeds

We observe that , while the Interestingly, while NDM and FKPP finds the Inferiortemporal region as the optimal seed, the Aβ-FKPP model finds the Entorhinal region as the optimal seed. We note here the lower α values, which could be attributable to the scalar impact of Aβ weights and actual difference in proportions of spread contribution.

Group	Model	Seed	α	r
CN	NDM	Inf. temporal	–	0.724
CN	FKPP	Inf. temporal	0.463	0.667
CN	Aβ-FKPP	Entorhinal	0.419	0.720
EMCI	NDM	Inf. temporal	–	0.719
EMCI	FKPP	Inf. temporal	0.448	0.663
EMCI	Aβ-FKPP	Entorhinal	0.433	0.713
LMCI	NDM	Inf. temporal	–	0.718
LMCI	FKPP	Inf. temporal	0.467	0.654
LMCI	Aβ-FKPP	Entorhinal	0.419	0.709
AD	NDM	Inf. temporal	–	0.717
AD	FKPP	Inf. temporal	0.450	0.662
AD	Aβ-FKPP	Entorhinal	0.409	0.712

Table 2: Comparison of models across clinical groups and seed regions

3.3.2 Residuals by Region

From Figure **??**, the NDM model indeed exhibits a stronger linear relationship between prediction and target values.

We highlight the 3 regions with the largest overpredictions and underpredictions in Figure **??**. All 3 models had similarly had largest overpredictions for the Transeversetemporal regions on both sides. We found a distinction between the NDM and FKPP models versus the Aβ-FKPP model on the underpredictions. The NDM and FKPP models had the largest underprediction for the Lateralorbitofrontal regions on both sides, while the Aβ-FKPP model had the largest underprediction for Inferiortemporal regions on both sides, which, interestingly, corresponds to the optimal seed region for both NDM and FKPP models.

3.3.3 Robustness testing through individual connectome analysis

Though the NDM fit to group average connectome had better r values, we observed that the mean performance across individuals had the largest (negative) difference compared to other models, and had the largest 95 percentile ranges. The NDM also had the largest 95 percentile range of SSE values across individuals, indicating that the model fit was not robust across individuals.
Aβ-FKPP model had generally worse performance mean across individuals, but this may be attributable to using group-averaged Aβ-FKPP values that aligned better with group-averaged connectomes, and it would be interesting to see if the model fit improves when using individual Aβ-FKPP values.

3.4 Using optimal hyperparameters from the Aβ-FKPP model on FKPP

The FKPP model, when forced to use the Aβ-FKPP model's optimal parameters, sees an increase in SSE from 1.86 to 2.40, and a decrease in r score from 0.72 to 0.62. We see an increase in predicted tau deposition in the Precentral and Postcentral regions, but a decrease in Bankssts and the Inferiortemporal regions. This divergence from pure FKPP suggests that the Aβ-modulated seed choice and growth rate emphasize certain pathways in a way that does not neatly translate into the unweighted FKPP environment. These findings underscore that parameters valid in a model incorporating amyloid load may not fully transfer to a simpler model, highlighting the importance of explicitly accounting for amyloid–tau interactions to

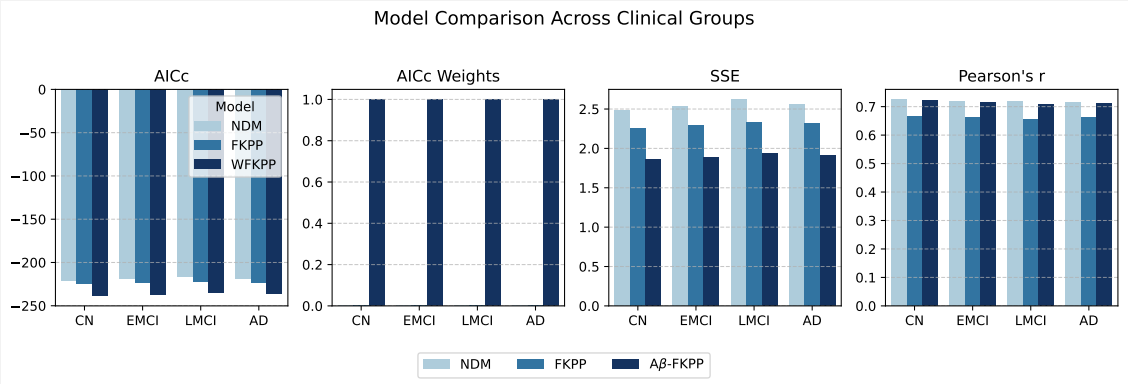

(a) *Comparison of model performance across different cognitive stages.*

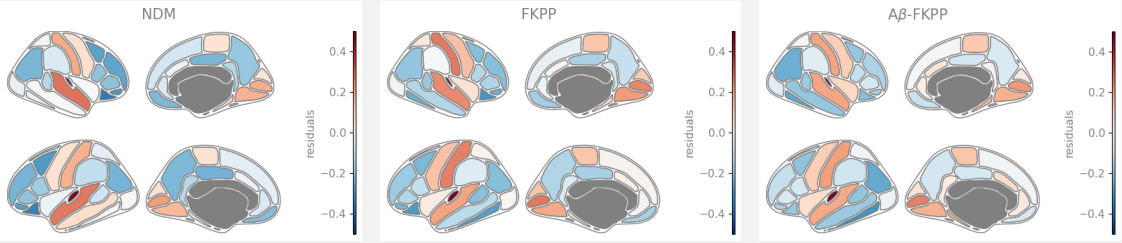

(b) **(c)** **(d)**

Residuals from NDM, FKPP, Aβ-FKPP on the cortical surface in CN.

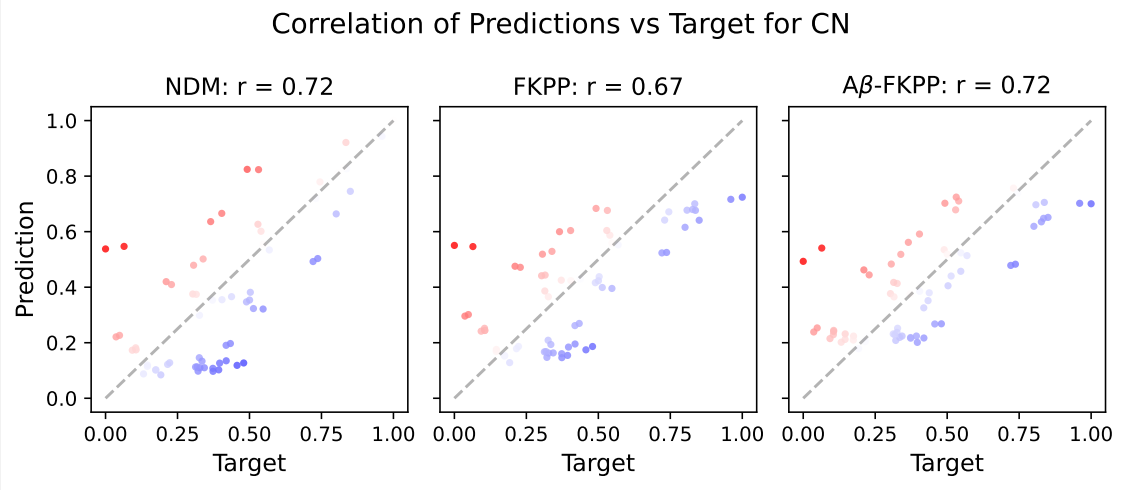

(e) *Prediction vs target for NDM, FKPP, and Aβ-FKPP models in CN.*

	NDM	FKPP	WFKPP
Over	Transversetemporal R Transversetemporal L Temporalpole R	Transversetemporal R Transversetemporal L Pericalcarine L	Transversetemporal R Transversetemporal L Pericalcarine L
Under	Lateralorbitofrontal R Lateralorbitofrontal L Parsorbitalis R	Lateralorbitofrontal R Lateralorbitofrontal L Inferiortemporal L	Inferiortemporal L Inferiortemporal R Inferiorparietal L

Figure 4: Regions with largest prediction errors across models in CN group

Table 3: Model performance distribution across individual connectomes

Group	Model	SSE Avg	SSE Indiv. μ	SSE % diff	SSE 95p Range	Pearson's r Avg	Pearson's r Indiv. μ	Pearson's r % diff	Pearson's r 95p Range
CN	NDM	2.48	2.50	0.64	0.555	0.724	0.677	**-6.97**	0.168
CN	FKPP	2.25	2.26	0.45	0.352	0.667	0.655	-1.69	0.091
CN	Aβ-FKPP	1.86	1.90	**2.14**	0.394	0.720	0.718	-0.36	0.151
EMCI	NDM	2.53	2.56	1.04	**0.630**	0.719	0.686	-4.80	**0.174**
EMCI	FKPP	2.30	2.29	-0.36	0.348	0.663	0.654	-1.36	0.091
EMCI	Aβ-FKPP	1.88	1.92	1.90	0.453	0.713	0.715	0.20	0.113
LMCI	NDM	2.62	2.60	-0.53	0.604	0.718	0.654	**-9.76**	**0.174**
LMCI	FKPP	2.33	2.35	0.83	0.468	0.654	0.641	-2.03	0.110
LMCI	Aβ-FKPP	1.93	1.96	1.44	**0.662**	0.709	0.706	-0.43	0.141
AD	NDM	2.56	2.61	**1.87**	**0.809**	0.714	0.656	**-8.97**	**0.231**
AD	FKPP	2.32	2.32	0.16	0.505	0.662	0.645	-2.69	0.126
AD	Aβ-FKPP	1.91	1.95	**2.09**	0.426	0.712	0.708	-0.58	0.116

better capture disease progression patterns.

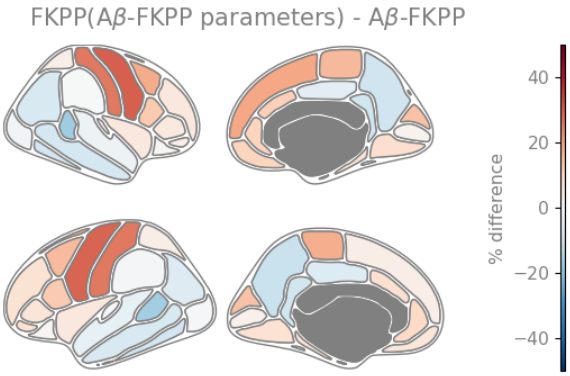

(a) Prediction difference between FKPP with Aβ parameters versus Aβ-FKPP.

	Regions	% Diff
FKPP higher	Precentral L	29.7
	Postcentral L	29.2
	Precentral R	26.4
Aβ-FKPP higher	Bankssts L	17.6
	Bankssts R	17.2
	Inferiortemporal R	11.2

(b) Top 3 regions with largest differences between models

3.5 Influence of Aβ on tau production

The null model performs significantly worse (permutation-based p-value < 0.01), thus concluding that ground truth Aβ is the key factor for Aβ-FKPP's performance. What's most interesting is the inclination towards Inferiortemporal regions as the optimal seed, which corresponds also to the optimal seeds in NDM and FKPP models, meanwhile the original Entorhinal seed was never selected.

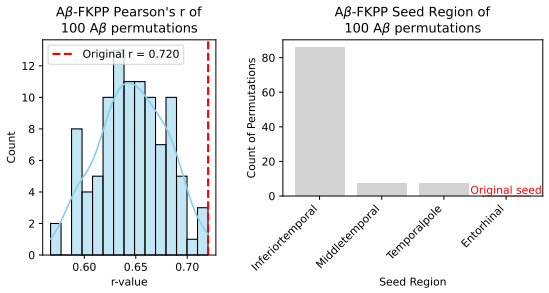

(a) **(b)**

Figure 6: Distribution of r values when permuting the Aβ weights (a) and The distribution of optimal seed regions across 100 permutations (b).

3.6 The effect of the best performing cognitive group on FKPP and NDM

In both FKPP and NDM, the null models perform significantly worse, with the best connectome a large margin away from the original, thus verifying that the original connectome is a key factor for the best performing group average connectome's performance. We also see a more diverse set of optimal seed regions chosen.

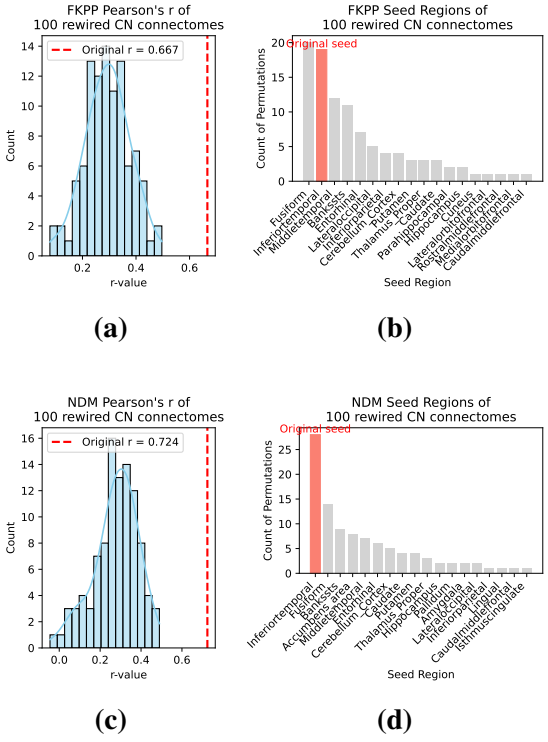

Figure 7: Distribution of r values when rewiring connectomes (a) and The distribution of optimal seed regions across 100 permutations (b).

4 Discussion

References

Davina Biel, Ying Luan, Matthias Brendel, Paul Hager, Anna Dewenter, Alexis Moscoso, Diana Otero Svaldi, Ixavier A. Higgins, Michael Pontecorvo, Sebastian Römer, Anna Steward, Anna Rubinski, Lukai Zheng, Michael Schöll, Sergey Shcherbinin, Michael Ewers, Nicolai Franzmeier, and the Alzheimer's Disease Neuroimaging Initiative. 2022. Combining tau-PET and fMRI meta-analyses for patient-centered prediction of cognitive decline in Alzheimer's disease. *Alzheimer's Research & Therapy*, 14(1):166.

Michel Goedert. 2015. Alzheimer's and Parkinson's diseases: The prion concept in relation to assembled Aβ, tau, and α-synuclein. *Science*, 349(6248):1255555.

Tiantian He, Elinor Thompson, Anna Schroder, Neil P. Oxtoby, Ahmed Abdulaal, Frederik Barkhof, and Daniel C. Alexander. 2023. A coupled-mechanisms modelling framework for neurodegeneration.

Neil P. Oxtoby, Sara Garbarino, Nicholas C. Firth, Jason D. Warren, Jonathan M. Schott, Daniel C. Alexander, and For the Alzheimer's Disease Neuroimaging Initiative. 2017. Data-Driven Sequence of Changes to Anatomical Brain Connectivity in Sporadic Alzheimer's Disease. *Frontiers in Neurology*, 8.

Ashish Raj, Amy Kuceyeski, and Michael Weiner. 2012. A Network Diffusion Model of Disease Progression in Dementia. *Neuron*, 73(6):1204–1215.

Elinor Thompson, Anna Schroder, Tiantian He, Antoine Legouhy, Xin Zhao, James H. Cole, Neil P Oxtoby, and Daniel C Alexander. 2024. Demonstration of an open-source toolbox for network spreading models: Regional amyloid burden promotes tau production in Alzheimer's disease. *Alzheimer's & Dementia*, 20(S9):e093791.

František Váša and Bratislav Mišić. 2022. Null models in network neuroscience. *Nature Reviews Neuroscience*, 23(8):493–504.

Jacob W. Vogel, Nick Corriveau-Lecavalier, Nicolai Franzmeier, Joana B. Pereira, Jesse A. Brown, Anne Maass, Hugo Botha, William W. Seeley, Dani S. Bassett, David T. Jones, and Michael Ewers. 2023. Connectome-based modelling of neurodegenerative diseases: Towards precision medicine and mechanistic insight. *Nature Reviews Neuroscience*, 24(10):620–639.

Johannes Weickenmeier, Mathias Jucker, Alain Goriely, and Ellen Kuhl. 2019. A physics-based model explains the prion-like features of neurodegeneration in Alzheimer's disease, Parkinson's disease, and amyotrophic lateral sclerosis. *Journal of the Mechanics and Physics of Solids*, 124:264–281.

Meichen Yu, Olaf Sporns, and Andrew J. Saykin. 2021. The human connectome in Alzheimer disease — relationship to biomarkers and genetics. *Nature Reviews Neurology*, 17(9):545–563.

A Appendix